EXTINCTION OF 10.6 μm LASER RADIATION BY FREE ELECTRONS IN AN ARGON DISCHARGE AT ATMOSPHERIC PRESSURE

BY

SEHYUN PARK

THESIS

Submitted in partial fulfillment of the requirements
for the degree of Master of Science in Electrical and Computer Engineering
in the Graduate College of the
University of Illinois at Urbana-Champaign, 2016

Urbana, Illinois

Adviser:

Professor J. Gary Eden

ABSTRACT

Experiments will be described in which the extinction of 10.6 μm photons by free electrons in a single filamentary discharge is studied. The extinction ranges from 3 to 10 percent over a path length of 1 cm, depending on the argon flow rate. The spatio-temporally averaged electron density in the filament is more than 10^{15} cm^{-3}, as determined by Stark broadening of the hydrogen alpha (656.28 nm) and 4p'[$\frac{1}{2}$]-4s[$\frac{3}{2}$]^0 argon I (696.54 nm) lines. Experiments indicate that the observed extinction of 10.6 μm is attributable to a combination of inverse bremsstrahlung and a negative lens effect, and the results will be compared to theoretical calculations based on Boltzmanns equation. The potential application of such high electron density plasmas to studies of fundamental plasma phenomena, as well as optical applications, will be discussed.

To my family, for their love and support.

ACKNOWLEDGMENTS

I would first like to express my sincere appreciation to Professor Gary Eden for his support and insight that he has given me. I also thank Professor Sung-Jin Park for his guidance and advice on the project. This thesis work has an important meaning to me not only because the project is enjoyable, but also because I could work together with my colleagues at the Laboratory for Optical Physics and Engineering (LOPE). All the fabrication skills and laboratory techniques I learned from Hee Jun are one of the important assets I have obtained in the lab. I give my deepest gratitude to Chul who first taught me how to operate microplasma devices. I very much appreciate Thomas Houlahan for teaching me how to use a spectrometer system and advice on the project. Thank you, Andrey, for the knowledge and the help on setting up optics for the attenuation experiment. I will miss you and the time spent with you playing with capillary tubes, Kyle. I also show my gratitude to all my colleagues in the lab for the great time we had together.

I am grateful to my grandparents and my father for their infinite love. I thank my aunt, uncles, and cousins for their support. I always feel very fortunate that I have such a wonderful family.

TABLE OF CONTENTS

CHAPTER 1

INTRODUCTION

Inverse bremsstrahlung is one of the most fundamental processes in optics and plasmas. In the process, the absorption of a photon occurs during a collision with a free electron under the influence of a neutral atom or ion. The photon energy absorbed is converted into the thermal energy of the electron which results in the increase in electron temperature. Just like the bremsstrahlung process, inverse bremsstrahlung is often dealt with in high temperature thermal plasma, such as fusion plasma, because of its linear dependency of gas pressure and electron density. However, it has been shown that the process is feasible in low temperature plasma cases [1], and it opens up interesting possibilities such as optical limiting applications along with the practical characteristics of low-temperature plasmas.

The theoretical background has been established using the Boltzmann kinetic equation [2]. It was also demonstrated that quantum corrections should be included when the electron velocity is comparable to the speed of light. Experimental studies were also conducted in various ways. Due to its nature, the process is typically observed in laser-induced plasmas [3], [4]. Zamir *et al.* [1] showed that absorption of 10.6 μm photons from a CO_2 laser occurs in high pressure electron-beam excited xenon plasmas. It was also noted that the slow component for the decay of electron density is governed by electron relaxation by collisions between excimer species. Fabre *et al.* presented that absorption increases sharply at the critical electron density [5]. In view of applications, there have been trials to use this phenomenon as a method to measure electron density of the plasma system because of its strong dependency of the inverse bremsstrahlung absoroption coefficient on electron density [3].

Although there have been many investigations to understand the phenomenon described above, some parameters, such as an inverse bremsstrahlung cross-section, are still poorly understood. In this thesis, a filamentary dis-

charge occurring within a capillary dielectric barrier discharge (DBD) device will be utilized as a tool to investigate the inverse bremsstrahlung process. In the experiment, the plasma device is probed by Stark broadening of the H_α line (656.28 nm) and the 4p'$[\frac{1}{2}]$-4s$[\frac{3}{2}]^0$ Ar I line (696.54 nm), and by CO_2 laser absorption. In Chapter 2, important parameters for the wave-plasma interaction will first be given first. The inverse bremsstrahlung absorption coefficient will be derived and there will be a brief description of a filamentary discharge. The theory for Stark broadening will be established in Section 2.4. After an illustration of the experimental setup, the results of electron density measurement and attenuation experiments will be discussed.

CHAPTER 2

THEORETICAL BACKGROUND

2.1 Wave-Plasma Interaction

The plasma frequency is the speed at which the ionized medium reacts to an external electromagnetic perturbation. The expression for the plasma frequency is easily derivable from a conceptual situation as follows. Assuming ions are immobile as compared to mobile electrons, an instantaneous electric field causes a charge density shift in the direction of the electric field. Then, electrons and ions will move toward each other to compensate for the charge imbalance. In this given situation, the plasma frequency can be obtained from a second order differential equation [6].

$$\omega_p = \sqrt{\frac{n_e e^2}{m\epsilon}} \tag{2.1}$$

where m is the electron mass.

When the interaction between an external electromagnetic wave and the collisionless plasma is described, the plasma frequency can be considered as a cut-off frequency that determines whether the wave is propagating through the medium or not. For a transverse electromagnetic wave in collisionless plasma, the dispersion relation is written as [6],

$$k = \frac{\omega}{c}\sqrt{1 - \frac{\omega_p^2}{\omega^2}} \tag{2.2}$$

Although this expression is only applied to collisionless plasmas, it gives the basic ideas about the interaction between plasmas and electromagnetic waves along with the plasma frequency. A more detailed analysis including collisions will be presented later in the following section.

2.2 Inverse Bremsstrahlung

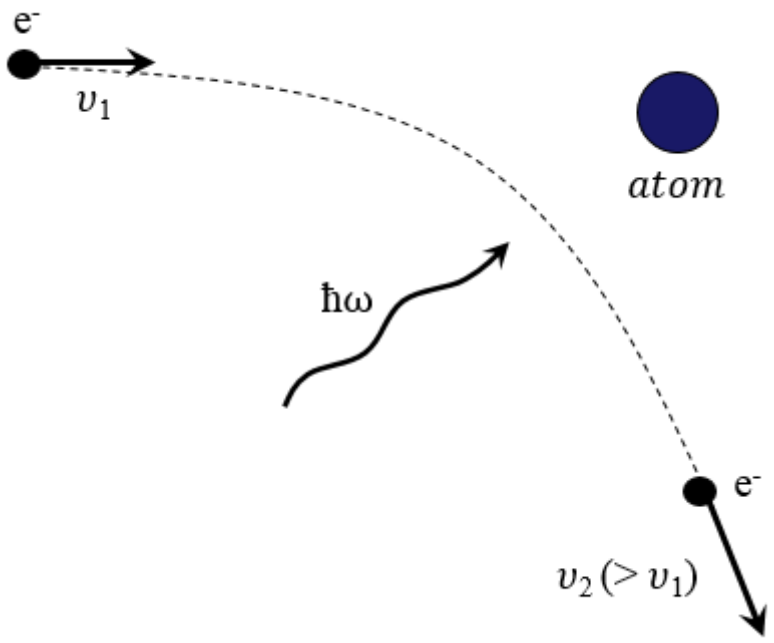

Figure 2.1: A schematic illustration of the inverse bremsstrahlung process at the atomic scale.

The primary mechanism for the inverse bremsstrahlung process in a weakly ionized plasma is attributed to collisions of electrons with neutral atoms as shown in Figure 2.1. In order to understand the behavior of a large number of particles, a statistical approach is necessary. For this purpose, distribution function, f_i, is defined in phase space that consists of six axes (r_x, r_y, r_z, v_x, v_y, v_z). The statistical behavior of particles is governed by the Boltzmann equation. When the electromagnetic force is dominant in the system, the Boltzmann equation is expressed as [6],

$$\frac{\partial f_i}{\partial t} + \mathbf{v} \cdot \frac{\partial f_i}{\partial \mathbf{r}} + \frac{e_i}{m_i}(\mathbf{E} + \mathbf{v} \times \mathbf{B}) \cdot \frac{\partial f_i}{\partial \mathbf{v}} = (\frac{\partial f_i}{\partial t})_{collisions} \tag{2.3}$$

With the assumption that the electron energy distribution function is well represented by a Maxwell-Boltzmann distribution, the effect of electron-neutral collisions can be regarded as a small perturbation caused by an RF

electromagnetic field [2],

$$f_i = f + f_1, \qquad E = E_0 + E_{rf} \tag{2.4}$$

where f is a time-stationary and isotropic distribution function whereas f_1 represents a small perturbation of the distribution function by an RF electromagnetic field. In a similar context, E_0 is an electrostatic field and E_{rf} is an RF electromagnetic perturbation. Since f is isotropic and time-stationary, $\frac{\partial f}{\partial t}$ and $\frac{\partial f}{\partial r}$ are zero. The magnetic term is negligible for a non-relativistic case. Also, the static field terms, E_0 and B_0, vanish. The decay rate for f_1 is assumed to be $\exp(-\nu_m(v)t)$ for the short-range electron-atom force [2]. Therefore, the Boltzmann equation simplifies to

$$\frac{\partial f_i}{\partial t} + \mathbf{v}\cdot \frac{\partial f_i}{\partial \mathbf{r}} + \frac{e}{m}\mathbf{E}_{rf}\cdot \frac{\partial f_i}{\partial \mathbf{v}} = -\nu_m(v) f_1 \tag{2.5}$$

where ν_m is the collision frequency for momentum transfer which is the frequency for elastic collisions between electrons and neutrals. Applying a Fourier-analysis and neglecting the term $k \cdot v$ in the present case, f_1 is expressed as,

$$f_1 = -\frac{e}{m}\frac{\frac{\partial f}{\partial \mathbf{v}} E_{rf}}{j\omega + \nu_m(v)} \tag{2.6}$$

The conductivity, then, is obtained from the distribution function by the relation,

$$\mathbf{J} = \sigma \cdot \mathbf{E}(\omega) = \Sigma_i q_i \int \mathbf{v} f_i d^3 v \tag{2.7}$$

In general electromagnetic theory, the relative permittivity for a lossy medium is related to conductivity,

$$\epsilon_r = 1 + \frac{\sigma}{j\omega\epsilon_0} \tag{2.8}$$

The resulting relative permittivity is

$$\epsilon_r = 1 + \frac{\omega_p^2}{\omega}\int_0^\infty (\frac{\omega + j\nu_m}{\omega^2 + \nu_m^2})\frac{\partial f}{\partial v}\frac{4\pi}{3} v^3 dv \tag{2.9}$$

The absorption coefficient is obtained from the dispersion relation by the expression [7],

$$\alpha = -2 \times Im(k) = -\frac{\omega}{c}\frac{Im(\epsilon_r)}{n} \tag{2.10}$$

Finally, the absorption coefficient is

$$\alpha(\omega) = -\frac{1}{n}\frac{4\pi}{3}(\frac{\omega_p}{\omega})^2 \int_0^\infty \frac{\nu_m(v)}{1+(\frac{\nu_{m(v)}}{\omega})^2}\mathbf{v}^3\frac{\partial f(v)}{\partial v}dv \tag{2.11}$$

where n is the real part of refractive index, ω_p is the plasma frequency, ω is the angular frequency of the electromagnetic perturbation, and ν_m is the collision frequency for momentum transfer.

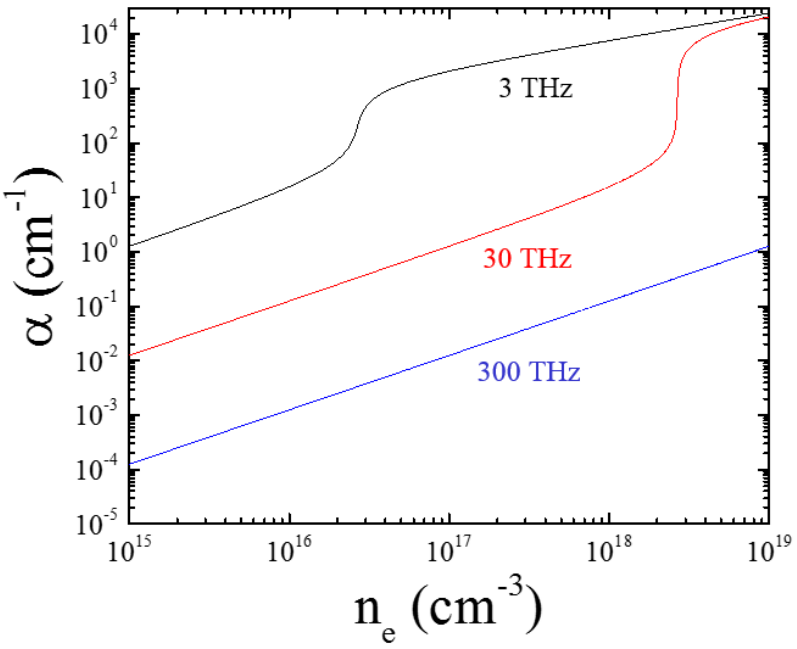

Figure 2.2: Inverse bremsstrahlung absorption coefficient versus electron density at three frequencies. Note that both axes are logarithmic.

The absorption coefficient is plotted versus electron density in Figure 2.2. The collision frequency for momentum transfer and electron temperature are assumed to be 10^{-12} s^{-1} and 2 eV, respectively.

Note that the absorption is linearly proportional to the electron density and the collision frequency when the collision frequency is assumed to be independent of velocity. The absorption from inverse bremsstrahlung is larger for filamentary discharges, as compared to typical macroscopic plasmas because of its high pressure operation and high electron density although a gemoetrical factor has to be considered. In the given pressure and angular frequency for electromagnetic field, the electron density plays a crucial role

in the determination of the absorption coefficient.

$$\alpha(\omega) \propto \frac{n_e \nu_m}{\omega^2} \tag{2.12}$$

The sudden increase in the absorption coefficient at a certain electron density is the result of the change in the real part of the refractive index. The sharp increase happens when the plasma frequency is equivalent to the angular frequency of electromagnetic wave. The electron density responsible for the abrupt transition can also be viewed as the critical plasma density which is readily derivable from the plasma frequency expression.

$$n_c = \frac{\epsilon_0 m_e}{e^2} \omega^2 \tag{2.13}$$

For example, the critical plasma density for an incident wave frequency of 30 THz in collisionless plasmas is $\sim 9.8 \times 10^{18}$ cm^{-3}, which is comparable to the value shown in Figure 2.2 of 3×10^{18} cm^{-3}.

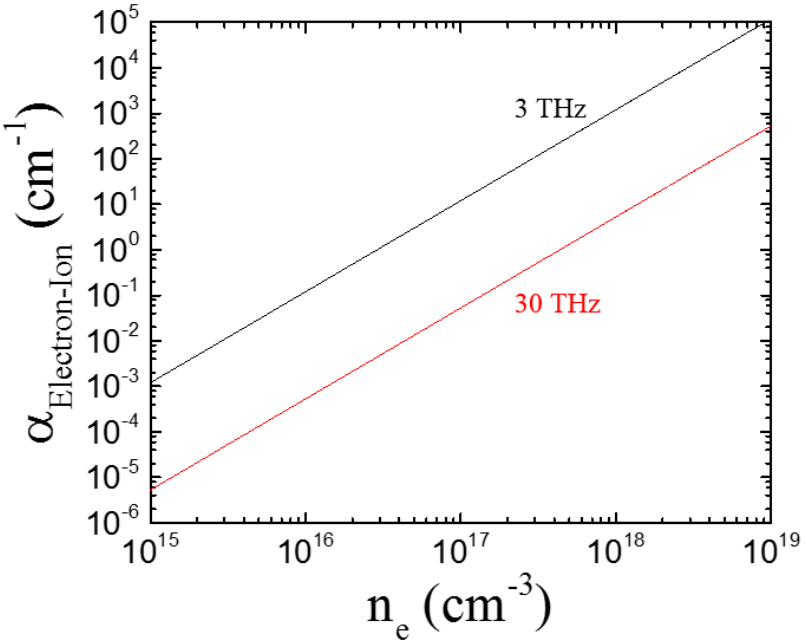

Figure 2.3: Inverse bremsstrahlung absorption coefficient for electron-ion interaction versus electron density of two frequencies. Both axes are logarithmic.

It should be noted that the ion-electron interaction is not negligible for electron densities higher than 10^{17} cm^{-3}. Figure 2.3 shows the absorption coefficient for electron-ion collisions versus electron density. Assuming the ion

density is the same as electron density, the ion-electron absorption coefficient [2] for an electron density of 10^{17} cm^{-3} is ~ 5 %-cm^{-1} which is non-negligible when compared to the absorption coefficient of the neutral atom-electron interactions.

The real part of the refractive index affects not only the absorption of the laser photons, but also the direction of the beam path. The gradient of the refractive index along the radial direction acts as a lens. Thus, the beam is deflected as it propagates through the plasma. The change of the refractive index by the electron density is shown in Figure 2.4.

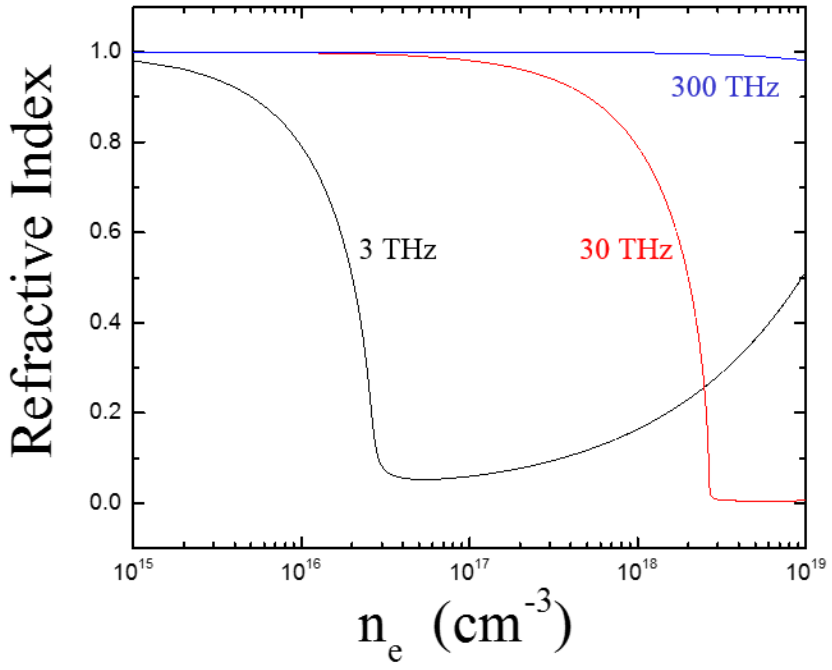

Figure 2.4: Real part of the refractive index versus the electron density at three frequencies.

2.3 Filamentary Discharge

Filamentation of diffusive glow discharges is thought to occur due to thermal instability, stepwise ionization, and Maxwellization [8]. The narrow channel shape is formed when the dominant mechanism for electron removal is a bulk recombination rather than diffusion to the wall. In this situation, the diffusion length of the electrons before they recombine is too short to reach

the wall. If a discharge occurs in inert gases, this typically implies that the main recombination mechanism is a dissociative recombination of dimer ions which is a fast recombination mechanism [9]. Understanding the mechanism is especially important to operate a laser system in which a diffusive glow discharge is preferred.

There have been many efforts to study the mechanism of the transition from a diffusive glow discharge to a filamentary discharge. Filamentary discharges typically occur at high pressure which is about atmospheric pressure [8]. Gherardi et al. have suggested that a gas flow can change the working domain of a filamentary discharge [10]. Also, the contraction of a diffusive glow discharge in neon gas has been observed by the author as the pressure increased from a few hundred Torr to a thousand Torr.

A filamentary discharge has characteristics which lie between those of a diffusive glow discharge and an arc discharge [8]. First, the electric field strength in a filamentary discharge is greater than that in an arc discharge but lower than that in a diffusive glow discharge. This is why a voltage drop is observed when a transition from a glow discharge to a filamentary discharge occurs. Second, a filamentary discharge is nonequilibrium plasma in the sense that the gas temperature is much lower than the electron temperature, but the gas temperature is still higher compared to that of a diffusive glow discharge. Lastly, the electron density is higher for a diffusive glow discharge, but lower for an arc discharge. The typical ionization ratio of a diffusive glow discharge is less than 10^{-6} while that for an arc discharge is 10^{-1} to 10^{-3}.

2.4 Stark Broadening

In order to determine a theoretical value for the inverse bremsstrahlung absorption coefficient, it is necessary to investigate the electron density of the plasma. As shown in Section 2.2, main factors that determine the inverse bremsstrahlung absorption coefficient are the electron density, the collision frequency, and the angular frequency of an electromagnetic wave. Among them, the collision frequency and the angular frequency are given in the experimental setup as 10^{12} s^{-1} and 30 THz, respectively. Once the electron density is obtained, the theoretical value for the absorption coefficient of inverse bremsstrahlung can be calculated.

In this thesis, a spectroscopic technique known as Stark broadening was employed to determine the electron density of the capillary plasma device. There have been many efforts to develop the technique to measure the electron density by observing a spectral line broadening of atoms or molecules [11], [12], [13], [14]. In a certain model where ions are stationary compared to electrons, the electric field felt by a probe species broadens the spectral lines of the species due to Stark effect. Especially, a Stark broadening technique that uses a hydrogen molecule as a probe species has been well established throughout decades [11], [13]. Furthermore, non-hydrogenic atoms have also been studied as a probe species for quadratic Stark broadening [12], [14], [15]. In this experiment, hydrogen gas is added for 1 $\%_{vol}$ as a probe molecule in argon background gas in order to investigate the broadening of the H_α line, 656.28 nm. The quadratic stark effect is examined using the 4p'$[\frac{1}{2}]$-4s$[\frac{3}{2}]^0$ Ar I line, 696.54 nm.

Since there are other types of line broadening mechanisms beside the Stark effect in the system, it is necessary to exclude the line broadenings of other mechanisms from the measured line width to obtain the broadening purely from the Stark effect. Broadening of the spectral line can be divided into two groups, which are Gaussian and Lorentzian [11]. Instrumental and Doppler broadening are responsible for the Gaussian component. The instrumental broadening is determined by the parameters of the spectrometer and the value is obtained as 0.02 nm from an Ar atomic line at 750.39 nm.

Doppler broadening results from the thermal motion of probe atoms relative to the observer. It is proportional to the gas temperature and inversely proportional to the mass of the atom. If the Maxwell-Boltzmann distribution is assumed, the broadening can be calculated using Equation 2.14 [12].

$$7.162 \times 10^{-7} \lambda \sqrt{\frac{T_h}{M}} \tag{2.14}$$

where λ is a wavelength of the photon emitted, T_h is a gas temperature, and M is a mass of the atom.

There are two types of pressure broadenings, van der Waals and Stark broadening, which are responsible for the Lorentizan component. Van der Waals broadening is caused by a dipolar interaction of probe atoms with neutral perturbers. The broadening can be obtained from Equation 2.15

[12], [16].

$$8.18 \times 10^{-26} \lambda^2 (\alpha R^2)^{2/5} (\frac{T}{\mu})^{3/10} N \tag{2.15}$$

where $R^2 = R_i^2 - R_f^2$, $R_j^2 = \frac{n^2}{2}[5n^2 + 1 - 3l_j(l_j + 1)]$, and $n = (\frac{E_H}{E_{ion} - E_j})^{1/2}$. Finally, the Stark broadening component is obtained by subtracting other broadenings from a measured line width.

CHAPTER 3

EXPERIMENTAL ARRANGEMENT

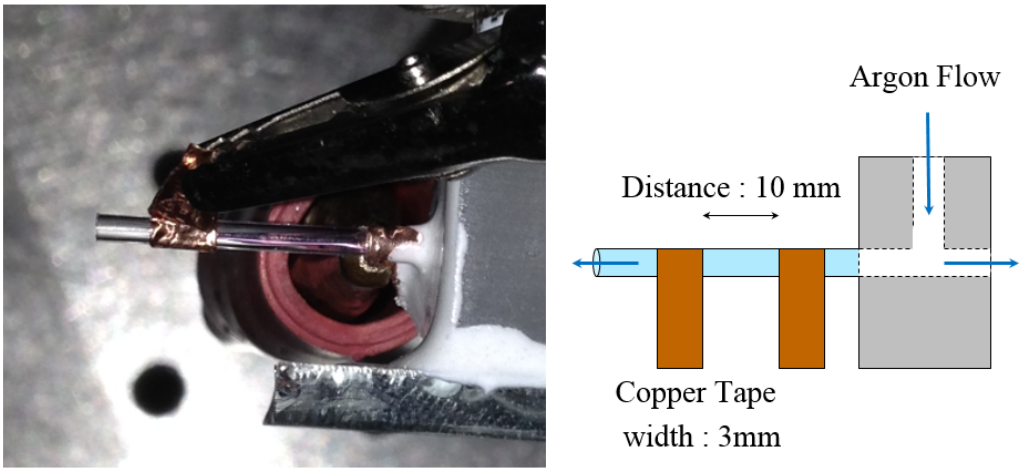

Figure 3.1: A picture of an operating device (left). A drawing showing the structure of the device (right).

The left portion of Figure 3.1 is a picture of an operating device. A single filament is observed in the center of the capillary. The right half at the figure is a simplified drawing of the device structure. The diameter of the capillary is 1.1 mm. The capillary wall is made of borosilicate, which acts as a dielectric, has a thickness of 100 μm. Copper tape is wound around the borosilicate capillary and serves as the electrodes. The capillary is bound by thermal epoxy to the polypropylene body. A research grade argon flow introduced to the microcavity is controlled by a mass flow controller. A waveform generator, an audio amplifer, and a transformer produce a 20 kHz sinusoidal voltage as large as 3.2 kV_{rms} to the device. The waveform is shown in Figure 3.2 for four different argon flow rate.

The experimental arrangement for the photon absorption studies is shown in Figure 3.3. A 400 mW CO_2 laser was chosen as a light source. The wavelength range of the laser is 10.3-10.8 μm and the beam waist is 2.4 mm while its divergence is 5.5 mrad. The laser beam was chopped by a 1 kHz

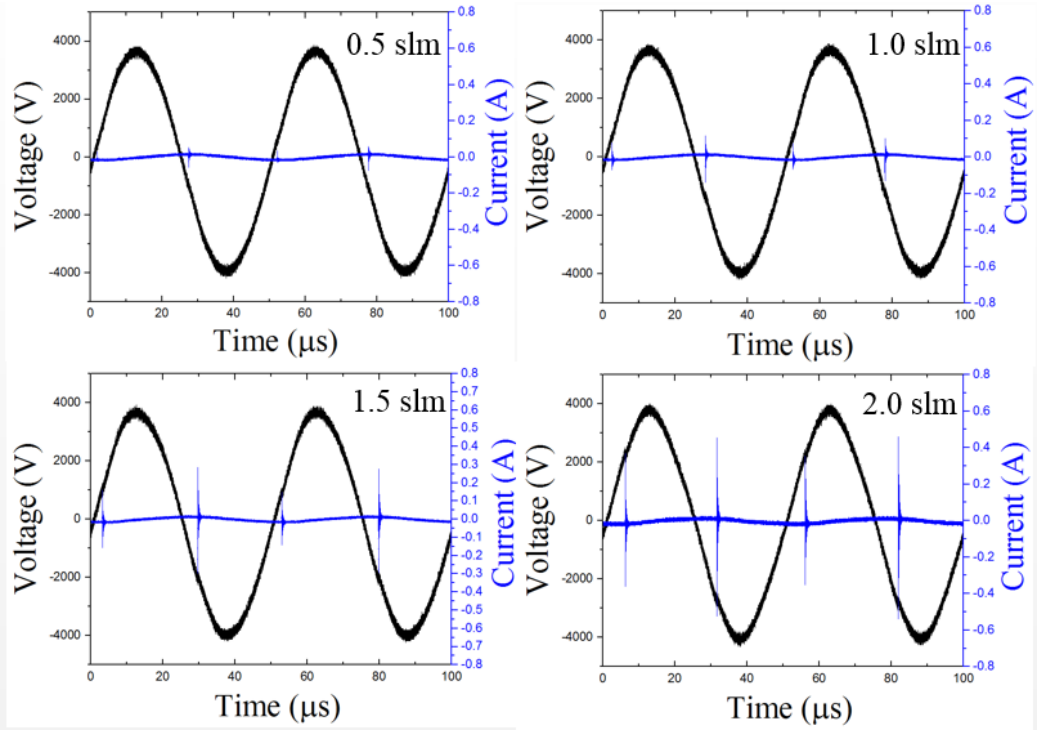

Figure 3.2: Waveforms for a capillary device for argon flow rate of 0.5 slm, 1 slm, 1.5 slm, and 2 slm from left-top corner to right-bottom.

mechanical chopper to prevent overheating the IR detector. The IR detector module includes a HgCdTe (MCT) detector, a built-in preamplifier, and a thermoelectrical cooling unit. The spectral response of the detector ranges from 2.5 to 11 μm, and the frequency response bandwidth of the module is 500 kHz. ZnSe lenses were used to focus the laser beam to the device and collimate the beam prior to reaching the detector. Two mirrors were placed between the CO_2 laser and the device to control the beam path precisely.

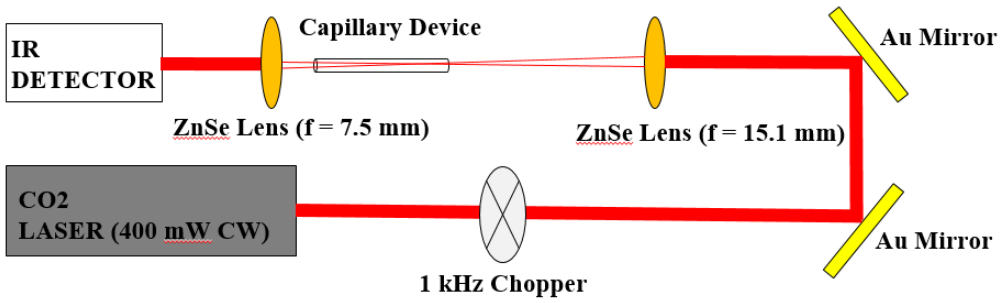

Figure 3.3: Experimental arrangement to observe extinction of a 10.6 μm photon by a capillary plasma device.

A Czerny-Turner type spectrometer equipped with an intensified charge-coupled device (ICCD) camera was utilized to observe the broadening of the hydrogen and argon lines for the electron density measurements. The focal length of the spectrometer and the slit width are 0.75 m and 20 μm, respectively. The groove density for the diffraction grating is 1800 mm^{-1} and the blazing wavelength is 500 nm. The resulting resolution of 0.02 nm was experimentally determined from observation of an Ar atomic line at 750.39 nm.

CHAPTER 4

RESULTS AND DISCUSSION

4.1 Electron Density Measurement

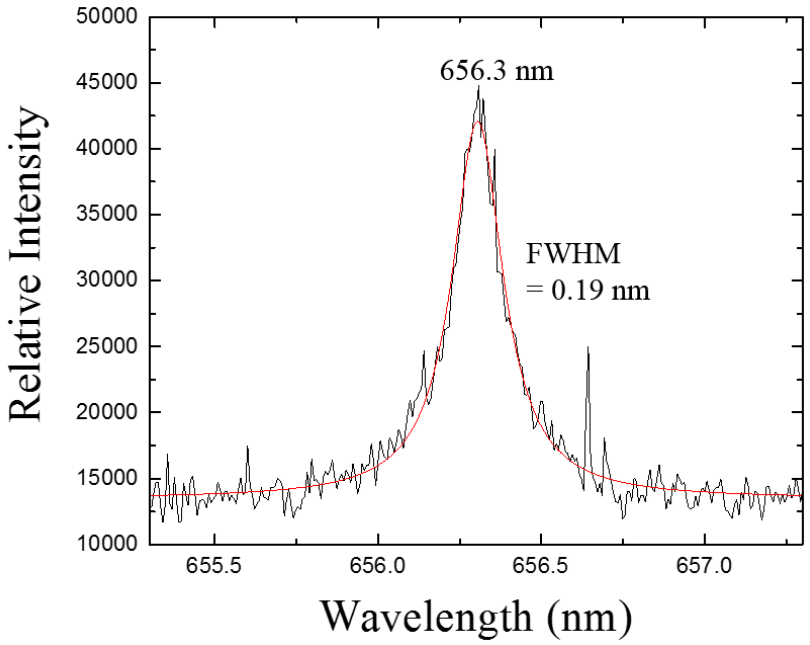

Figure 4.1: Spectral broadening of the H_α line, at 656.28 nm. The red line represents the fitting of a Lorentzian.

Figure 4.1 shows the full width at half maximum (FWHM) of the H_α line for 2 slm argon flow and less than 1% of hydrogen gas added to the feedstock Ar. The red line shows a Lorentzian fitting. The Doppler broadening is calculated from Equation 2.14 to be 0.015 nm for a gas temperature of 1000 K. Considering the dipole moment of a hydrogen atom and atomic polarizability of argon, the van der Waals broadening is calculated from Equation 2.15 as 0.049 nm at 760 Torr and 1000 K. The total line width is measured to be 0.19 nm and the resulting Stark broadening after the deduction is 0.106

nm. Tabulated values [13] give a measured electron density of approximately 2×10^{15} cm^{-3} at an electron temperature of 10,000 K.

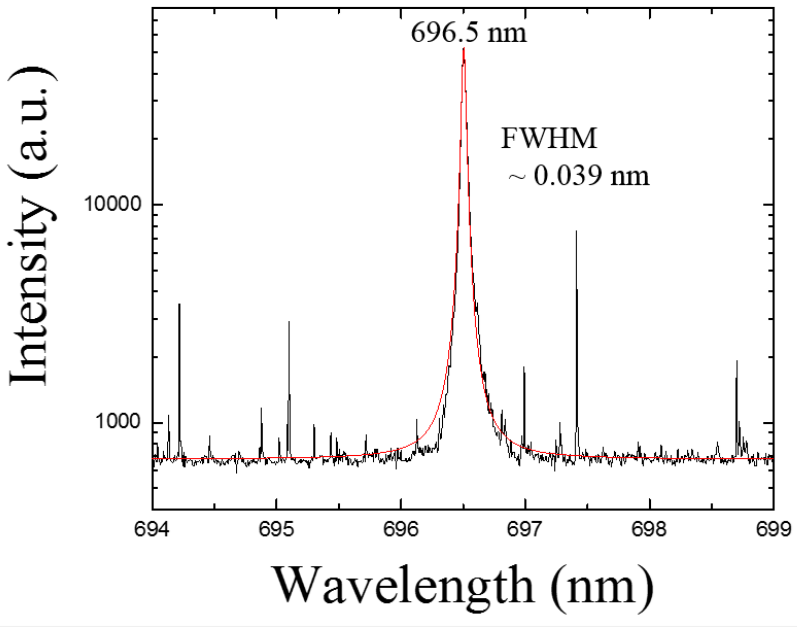

Figure 4.2: Spectral broadening of argon I line, 696.54 nm. The red line represents the fitting of a Lorentzian.

Ar I line broadening is also investigated in order to confirm the electron density obtained from the H_α line. Figure 4.2 shows the 4p'[$\frac{1}{2}$]-4s[$\frac{3}{2}$]^0 Ar I line and Lorentzian fitting to it at a 2 slm argon flow rate. Applying the similar procedure done for H_α, the Doppler broadening and van der Waals broadening calculated from Equations 2.14 and 2.15 are 0.003 nm and 0.012 nm, respectively. The total line width is measured as 0.039 nm. As a result, the stark broadening is 0.004 nm. The electron density is approximately 3.6×10^{15} cm^{-3} at an electron temperature of 10,000 K [12], [14].

The inconsistency in electron density measurement could result from a resolution limit of the spectrometer. Especially when the broadening of Ar I line was measured, the measured Stark width was 0.004 nm while the error range of the value was 0.002 nm. The instrumental broadening also has the same error range. Furthermore, there is a decrease in the H number density because of ionization when the electron density is high while the neutral argon density remains almost constant [18]. This implies that radiation from hydrogen atoms mostly comes from when the electron density is small. The assumption made for gas and electron temperature which have not been

measured experimentally could also result in the inconsistency.

4.2 Attenuation Experiment

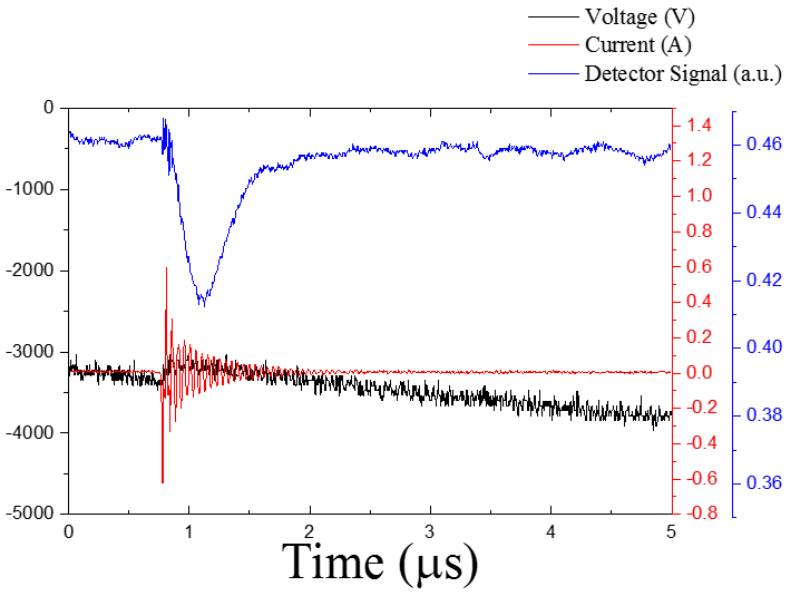

Figure 4.3: Magnified view of the detector signal, voltage, and current.

Figure 4.3 shows the voltage, current and detector signal when a discharge occurs at a 2 slm argon flow rate. A slight decrease in the magnitude of the voltage and a ringing of the current are observed. Strong noise at the beginning of the extinction of detector signal at around 800 ns in Figure 4.3 results from an electromagnetic field interference produced from the discharge. The extinction occurs within 300 ns and it rises again within 1 μs, but these rise and fall times are limited by the temporal response of the detector specification. The maximum extinction ratio is linearly proportional to the root mean square (RMS) current as shown in Figure 4.4. This result is plausible because the magnitude of the current is proportional to the electron density which affects the extinction ratio. Furthermore, the current peak tends to have a greater magnitude in the negative half cycle of the voltage which is indicated in the figure.

The maximum extinction which is approximately 12% of the total signal can be explained either by inverse bremsstrahlung or a negative lens effect, as discussed in Section 2.2. In order to calculate the theoretical value for

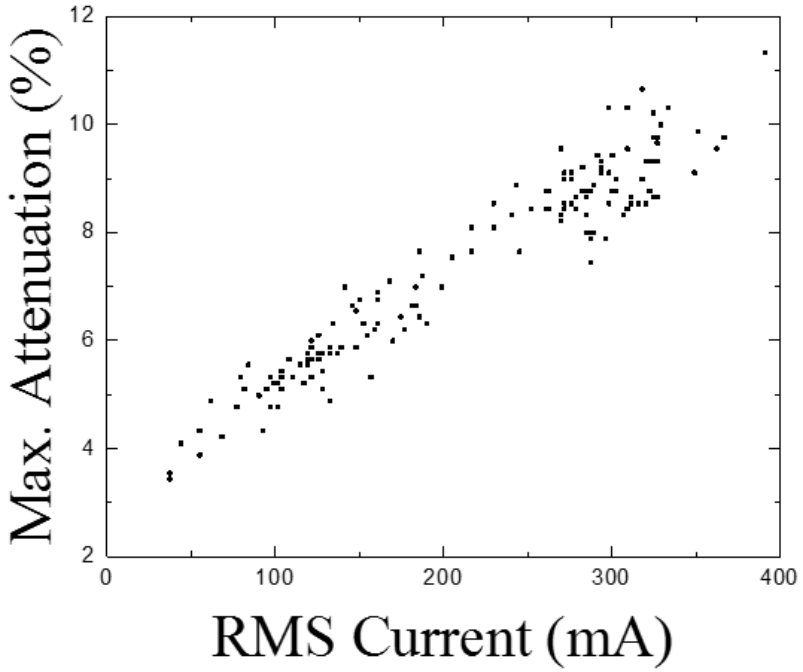

Figure 4.4: Maximum extinction versus the RMS current value.

absorption, it is necessary to obtain a filling factor of the plasma in the capillary tube. Figure 4.5 shows side and end-on views of the image obtained from an ICCD camera at argon flow rate of 2 slm. When the Gaussian shape is assumed for both the CO_2 laser beam and the intensity profile in the radial direction, the filling factor can be calculated from the FWHM of the plasma filament and the beam width. The resulting filling factor is approximately 0.09. Since the average extinction ratio is 10% at argon flow rate of 2 slm, this indicates that most of the photons passing through the plasma are either absorbed by either inverse bremsstrahlung absorption or deflected due to a negative lens effect.

Other possible mechanisms that may affect the photon extinction, such as a thermal lens effect and an ion thruster effect, were ruled out becuase they are typically very slow processes which take from microseconds to milliseconds [17]. Especially, a thermal lens effect has been observed by the author in an arc discharge in a cylinder-shaped device, and the fall time was approximately 100 ms. A reflection from the plasma and air interface is also possible, but the reflectance is less than 2×10^{-4} for an electron density of 10^{17} cm^{-3}.

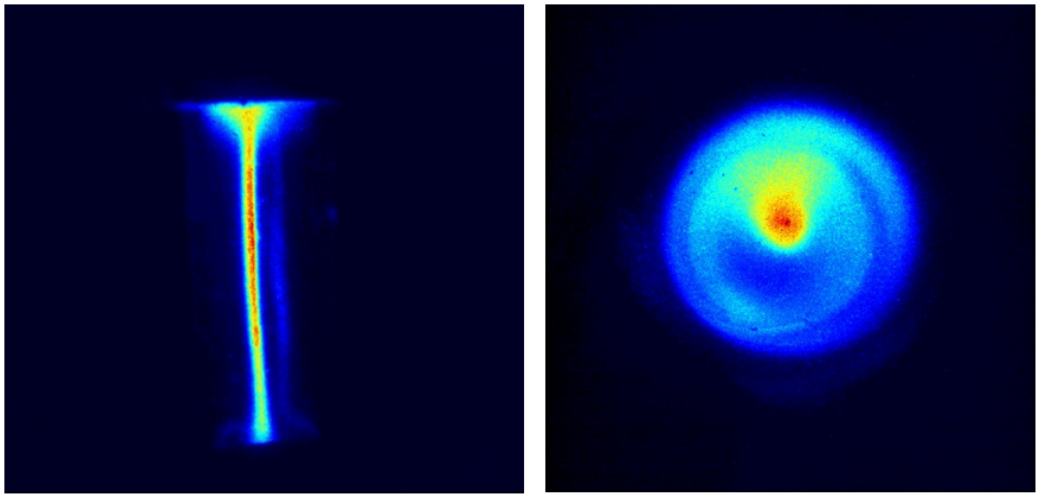

Figure 4.5: A side view (left) and an end-on view (right) of an ICCD image of the filamentary discharge.

CHAPTER 5

CONCLUSIONS AND FUTURE PLANS

An extinction of 10.6 μm photons by a filamentary discharge was observed. A theoretical background has been established for calculation of an absorption coefficient and a refractive index of plasma. The electron density of the plasma was obtained by spectral line broadenings of H_α and Ar I lines. At an argon flow rate of 2 slm, the average extinction for a negative half-cycle is 10%. The extinction is attributed to either inverse bremsstrahlung or a negative lens effect.

A further investigation is required to verify which mechanism is dominant for the extinction. Although a ZnSe lens is located between the plasma device and the detector to compensate for the deflection, it is difficult to exclude a negative lens effect totally. Thus, a more detailed theoretical study and experimental verification of the lens effect are required.

In order to make more apparent observations of inverse bremsstrahlung absorption, a glow discharge rather than a filamentary discharge is preferable because the filling factor is much more higher and negative lensing is of less consquence due to a smaller spatial gradient of the electron density. It is expected that short pulse voltage operation of the plasma device will produce many gas breakdowns at the same time so that the discharge becomes glow rather than filamentary [10], [18]. Cavity ring-down spectroscopy can also be utilized for a plasma with a small absorption coefficient [19].

Furthermore, a detector with a time constant less than a few nanoseconds needs to be used to examine the inverse bremsstrahlung cross-section as well as rate constants of the reactions occurring in the discharge.

REFERENCES

[1] E. Zamir, C. W. Werner, W. P. Lapatovich, and E. V. George, "Temporal evolution of the electron density in high-pressure electron-beam-excited xenon plasmas," *Appl. Phys.Lett.*, vol. 27, no. 2, pp. 56-58, 1975.

[2] G. Bekefi, *Radiation Processes in Plasmas*, New York, NY: John Wiley & Sons, 1979.

[3] A. A. Offenberger, R. D. Kerr, and P. R. Smy, "Plasma diagnostics using CO_2 laser absorption and interferometry," *J. Appl. Phys*, vol. 43, no. 2, pp. 574-577, 1971.

[4] L. Schlessinger and J. Wright, "Inverse-bremsstrahlung absorption rate in an intense laser field," *Phys. Rev. A.*, vol. 20, no. 5, pp. 1934-1945, 1979.

[5] E. Fabre and C. Stenz, "CO_2-laser beam absorption by a dense plasma," *Phys. Rev.*, vol. 32, no. 15, pp. 823-826, 1973.

[6] B. E. Cherrington, *Gaseous Electronics and Gas Lasers*, Elmsford, NY: Pergamon Press, 1979.

[7] S. L. Chuang, *Physics of Photonic Devcies*, 2nd ed. Hoboken, NJ: Wiley & Sons, 2009.

[8] Y. P. Raizer, *Gas Discharge Physics*, Berlin, Germany: Springer-Verlag, 1991.

[9] H. J. Qskam and V. R. Mittelstadt, "Recombination coefficient of molecular rare-gas ions," *Phys. Rev.*, vol. 132, no. 4, pp. 1445-1454, 1963.

[10] N. Gherardi and F. Massines, "Mechanisms controlling the transition from glow silent discharge to streamer discharge in nitrogen," *IEEE Trans. Plasma Sci.*, vol. 29, no. 3, pp. 536-544, 2001.

[11] H. Griem, *Principles of Plasma Spectroscopy*, New York, NY: Cambridge University Press, 1997.

[12] S. Djurovic and N. Konjevic, "On the use of non-hydrogenic spectral lines for low electron density and high pressure plasma diagnostics," *Plasma Sources Sci. Technol.*, vol. 18, p. 035011, 2009.

[13] M. A. Gigosos and V. Cardenoso, "New plasma diagnosis table of hydrogen stark broadening including ion dynamics," *J.Phys. B: At. Mol. Opt. Phys.*, vol. 29, pp. 4795-4838, 1996.

[14] S. Pellerin, K. Musiol, B. Pokrzywka, and J. Chapelle, "Stark width of 4p'$[\frac{1}{2}]$-4s$[\frac{3}{2}]^0$ Ar I transition (696.543 nm)," *J. Phys. B: At. Mol. Opt. Phys.*, vol. 29, pp. 39113924, 1996.

[15] L. Dong, J. Ran, and Z. Mao, "Direct measurement of electron density in microdischarge at atmospheric pressure by Stark broadening," *Appl. Phys. Lett.*, vol. 86, p. 161501, 2005.

[16] C. S. Lee and D. M. Camm, "Van der Waals broadening of argon absorption lines," *J. Quant. Spectrosc. Radiat. Transfer.*, vol. 15, p. 211-216, 1975.

[17] A. Komuro and R. Ono, "Two-dimensional simulation of fast gas heating in an atmospheric pressure streamer discharge and humidity effects," *J. Phys. D: Appl. Phys.*, vol. 47, no. 15, p. 155202, 2014.

[18] D. Yarmolich, Y. E. Krasik, E. Stambulchik, V. Bernshtam, J. K. Yoon, B. Herrera, S.-J. Park, and J. G. Eden, "Self-pulsing 10^4 A cm^{-2} current density discharges in dielectric barrier Al/Al_2O_3 microplasma devices," *Appl. Phys. Lett.*, vol. 94, p. 011501, 2009.

[19] G. Berden, R. Peeters, and G. Meijer, "Cavity ring-down spectroscopy: Experimental schemes and applications," *Int. Reviews in Physical Chemistry*, vol. 19, no. 4, pp. 565-607, 2000.